High-temperature terahertz absorption band in rare-earth gallium garnet

Masaki Adachi,[1,*] Hiroaki Matsui,[1,2] Munetoshi Seki,[1] Hiroyasu Yamahara,[3] and Hitoshi Tabata[1,2,*]

[1]*Department of Electrical Engineering and Information Systems, Graduate School of Engineering, The University of Tokyo, 7-3-1 Hongo, Bunkyo-ku, Tokyo 113-8656, Japan*

[2]*Department of Bioengineering, Graduate School of Engineering, The University of Tokyo, 7-3-1 Hongo, Bunkyo-ku, Tokyo 113-8656, Japan*

[3]*Institute of Engineering Innovation, Graduate School of Engineering, The University of Tokyo, 7-3-1 Hongo, Bunkyo-ku, Tokyo 113-8656, Japan*

(Received 8 November 2014; revised manuscript received 23 January 2015; published 20 February 2015)

In addition to the absorption due to known optical phonons, we found a temperature-dependent absorption band at 2 THz in garnet-type $Ho_3Ga_5O_{12}$, at temperatures in the range of 450–540 K. The optical and electrical properties reveal that the absorption band at 2 THz is not produced by mechanisms related to soft phonons, rattling phonons, impurities, or charge density waves, but rather to polaron conduction. Our analysis of the scattering rates and optical mobility shows that electron transport via the intermediate polaron is significant in this absorption band. Electrical measurements also support the existence of polarons in $Ho_3Ga_5O_{12}$. This paper facilitates a method to investigate charge carrier transport from an optical point of view using terahertz time-domain spectroscopy, which we demonstrate using $Ho_3Ga_5O_{12}$.

DOI: 10.1103/PhysRevB.91.085118 PACS number(s): 78.47.D−, 63.20.kd, 72.80.Sk

I. INTRODUCTION

Terahertz time-domain spectroscopy (THz-TDS) is known to be a powerful tool for investigating the low-energy physics of inorganic materials [1,2], including electromagnons [3–5], charge density waves (CDWs) [6–8], and soft phonon modes [9,10]. These interesting optical properties in the THz region of the electromagnetic spectrum have been observed mainly at temperatures below 100 K [4–8]. The photon energy of the THz region of the electromagnetic spectrum is smaller than the thermal energy at room temperature (RT) (1 THz corresponds to a thermal energy of approximately 40 K). It is not straightforward to clearly observe the optical responses induced by THz pulses at temperatures above 300 K [11]. However, THz-TDS enables us to investigate low-energy physics in inorganic materials at temperatures above RT. We have previously reported THz-TDS analysis of garnet-type $Ho_3Ga_5O_{12}$ (HoGG) at RT. It was found that HoGG exhibited an optical phonon mode at 2.6 THz, with a very narrow spectral width [12]. Recently, we observed a broad absorption band at 2 THz, on the low-energy side of the lowest optical phonon mode at temperatures above 300 K. This absorption band was observed only over a narrow range of temperatures within from 450 to 540 K, and exhibited a peak at around 500 K. Similar behavior has been also reported in the THz regime in ferroelectric materials with soft mode phonons [9,10]. Soft mode phonons have been reported from lattice instabilities following heating to the Curie temperature [13]. In contrast, HoGG exhibits paraelectric behavior, which cannot be reasonably explained for the absorption band at 2 THz on the basis of soft phonon modes mechanisms applied for ferroelectric materials.

In this paper, we focus on the Debye temperature of HoGG, $\theta_D = 520$ K [14], which is close to the maximum temperature of the absorption band at 2 THz. In particular, the charge carrier transport around θ_D is characterized by hopping behavior, resulting in an increase in the mean-free path of electrons in the host [15]. So far, there have only been a few reports on carrier transport in rare-earth gallium garnets that considered polaron transport [16–18]; however, we believe that polaron conduction processes are important in producing the absorption band at 2 THz because of the relationship between the temperature dependence of the optical and electrical properties, which is discussed in this paper. We report a temperature-dependent absorption band at 2 THz, which is attributed to polaron charge carrier transport in HoGG. The absorption band was observed only at temperatures in the range of 450–540 K. We provide a theoretical analysis of the origin of carrier conduction in HoGG. It is not straightforward to determine the origin of charge carrier transport in highly insulating materials; however, THz-TDS allows us to obtain information regarding charge carrier transport that cannot be obtained using electrical measurements, and which is demonstrated using a highly insulating garnet material HoGG.

II. EXPERIMENTAL

$Ho_3Ga_5O_{12}$ polycrystalline samples were synthesized using a solid-state reaction technique. Ho_2O_3 and Ga_2O_3 powders were mixed with stoichiometric compositions, and then pressed at 50 MPa in vacuum to form pellet samples. These pellets were sintered at 1200 °C for 10 h in air (at a cooling rate of 100 °C/h), reground, and then sintered again under the same conditions. The sintered pellets were polished by lapping to obtain a mirror plane for THz-TDS. All samples were 318 μm thick. X-ray diffraction (XRD) analysis revealed that all samples had a single phase with a garnet structure. The mean grain size in the samples was approximately 1 μm, as determined using scanning electron microscopy (SEM) (JEM-2100F, JOEL Ltd.). Temperature-dependent THz-TDS measurements were carried out using a transmittance-type THz-TDS system (TAS7500SP, Advantest Ltd.). A conventional ceramic heater with a custom-made sample holder formed of aluminum with a 1-cm-diameter hole was used. The temperature-dependent electrical resistivity was measured using interdigitated Ohmic

*adachi@bioxide.t.u-tokyo.ac.jp; tabata@bioeng.t.u-tokyo.ac.jp

Pt electrodes (see the inset of Fig. 5). Energy dispersive x-ray spectroscopy (EDS) (JEM-2100F, JEOL Ltd.) was used to analyze the atomic composition.

III. RESULTS AND DISCUSSION

A. Complex dielectric function spectra

Figure 1 shows the complex dielectric function $\tilde{\varepsilon}$ obtained from the THz-TDS at different temperatures. The complex dielectric function $\tilde{\varepsilon}$ can be expressed using Lorentzian functions and a modified Debye model

$$\tilde{\varepsilon} = \varepsilon_\infty + \sum_{j=1}^{3} \frac{\Omega_j^2}{\left(\omega_{0j}^2 - \omega^2\right) - i\Gamma_j\omega} + \frac{\varepsilon_0 - \varepsilon_\infty}{1 + (i\omega\tau)^{1-\alpha}}, \quad (1)$$

where ε_0, ε_∞ is the permittivity constant in the static and high frequency limits, respectively; Ω_j is the oscillation strength; $f_{0j}(\omega_{0j}/2\pi)$ and Γ_j are the resonance THz frequency and the scattering rate of the jth resonant mode [19], respectively; ω is the angular frequency, and τ is the mean relaxation time; α indicates the distribution of relaxation times [20]. The three Lorentzian functions of the second term in Eq. (1) were used to perform spectral decompositions of an absorption band at 2 THz, lowest optical phonon mode at around 2.58 THz (phonon A) and background absorption based on 16 other phonon modes [21], respectively. In the third term, we employed a Cole-Cole relaxation model. It is known that rare-earth garnets show dielectric relaxations in the microwave range [20,22–23]. The increased Re $[\varepsilon_r]$ and Im $[\varepsilon_r]$ of real and imaginary parts in low frequency below 1 THz was attributed to dielectric relaxation-related phenomena, which can be expressed using a Cole-Cole relaxation model.

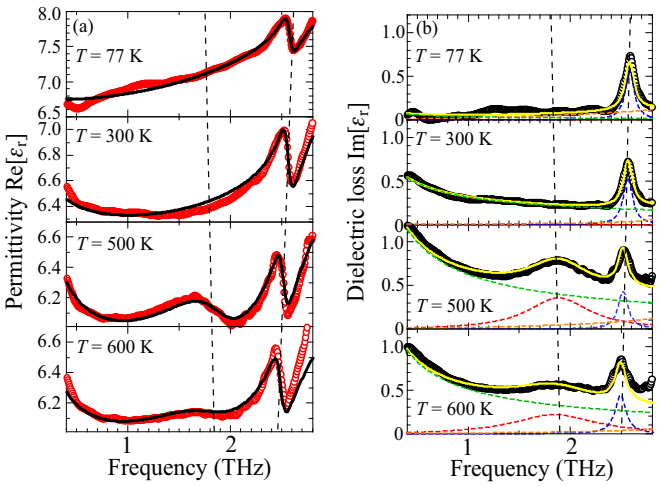

FIG. 1. (Color online) (a) Real part $\varepsilon'(\omega)$ and (b) imaginary $\varepsilon''(\omega)$ parts of complex dielectric functions in HoGG at 77, 300, 500, and 600 K. Red and black circles represent the experimental data in (a) and (b), respectively. Black and yellow lines indicate the parameter fits by Eq. (1) in (a) and (b), respectively. Blue and orange dotted lines are components of phonon A and background absorption in (b), respectively. Green dotted line shows a component of the dielectric relaxation in (b). Red dotted line shows a component of absorption band at 2 THz in (b).

TABLE I. Fitted parameters related to the optical loss spectra in HoGG.

Parameters	Fitted value
$\gamma_{G\|\mathrm{ph}-A}$	0.73
W_p (meV)	980
$\varepsilon_{\mathrm{def}}$ (eV)	22
α_s	2.96
m^* (m_e^{-1})	85.5

The results of parameter fits to the dielectric loss (Im $[\varepsilon_r]$) are shown in Figs. 1(a) and 1(b). Im $[\varepsilon_r]$ provided four kinds of absorption components, which could be also fitted to the permittivity, Re $[\varepsilon_r]$. The mean grain size in the polycrystalline HoGG samples was about 1 μm, which is significantly smaller than an incident wavelength of the THz radiation, so that the scattering component is not expected to be dominant in the whole temperatures, resulting in negligible contribution to the optical losses. The resonance frequencies $f_{0|\mathrm{ph}-A}$, associated with optical phonon A, gradually decreased with an increase of temperature, which obeyed the Grüneisen approximation as follows [24]:

$$\omega_p = \omega_{0|T=0} \exp\left[-3\gamma_G\left(\frac{a}{a_0} - 1\right)\right], \quad (2)$$

where $\omega_{0|T=0}$ is the resonance frequency at 0 K, and γ_G is the Grüneisen constant. Values of $\gamma_{G|\mathrm{ph}-A}$ in HoGG, associated with optical phonon A, were determined as 0.73 [see Table I], which was close to those of $Dy_3Fe_5O_{12}$ [24] and $Re_3Al_5O_{12}$ (Re: rare-earth ions) [25]. Temperature-dependent $\Gamma_{\mathrm{ph}-A}$ and $\Omega_{\mathrm{ph}-A}$ in HoGG were also similar to those in $Dy_3Fe_5O_{12}$ [24] [Figs. 2(b) and 2(c)]. On the other hand, the background absorption obeyed the Bose-Einstein statistics, as can be expressed by the following equation [26]:

$$n \propto \frac{\exp(\hbar\omega/k_BT)}{\exp(\hbar\omega/k_BT) - 1}, \quad (3)$$

where k_B is the Boltzmann constant. Figure 2(d) shows the temperature dependence of integrated intensity of background absorption normalized to that at 77 K, showing that the background absorption could be well fitted to Eq. (3) [orange dotted lines in Fig. 1(b)]. Furthermore, in a Cole-Cole relaxation model of Eq. (2), τ is expressed as a function of temperature by the following equation [20]:

$$\tau = \tau_0 \exp(E_a/k_BT), \quad (4)$$

where τ_0 and E_a is the Debye relaxation time and the activation energy, respectively. As shown in Fig. 2(e), temperature-dependent τ could be explained on the basis of Arrhenius law [green dotted lines in Fig. 1(b)]. The parameter fits to the optical phonons and dielectric relaxation were successfully extracted from the absorption component at 2 THz [red dotted lines in Fig. 1(b)].

B. Absorption band at 2 THz

Figure 3(a) shows oscillation strength Ω of the absorption band at 2 THz as a function of temperature. A value of Ω showed a peak structure of 0.70 in the vicinity of 500 K and

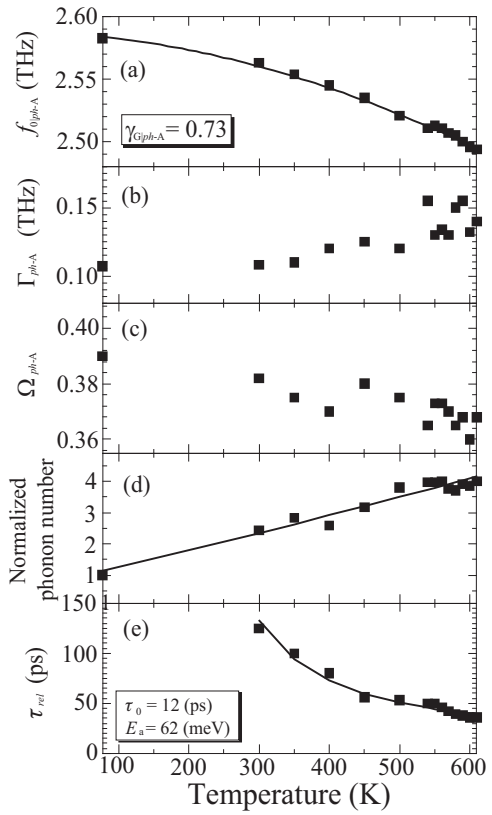

FIG. 2. Temperature dependence of (a) resonance frequency $f_{0|\mathrm{ph}-A}$, (b) scattering rate $\Gamma_{\mathrm{ph}-A}$, and (c) oscillation strength $\Omega_{\mathrm{ph}-A}$ for optical phonon A. A black square indicates experimental data for optical phonon A. Black line in (a) is a parameter fit to the Grüneisen approximation. (d) Temperature dependence of normalized phonon number in background absorption. Black line shows a parameter fit to the Bose-Einstein statistics. (e) Temperature dependence of relaxation time τ_{rel}. Black line shows a parameter fit to the Arrhenius law.

then decreased down to 0.35 at 600 K. A value of resonant frequency f_0 was shifted to high frequency with increasing temperature [Fig. 3(b)]. These temperature-dependent behaviors were different from those of optical phonon A. Figure 4(a) shows a scattering rate Γ as a function of temperature,

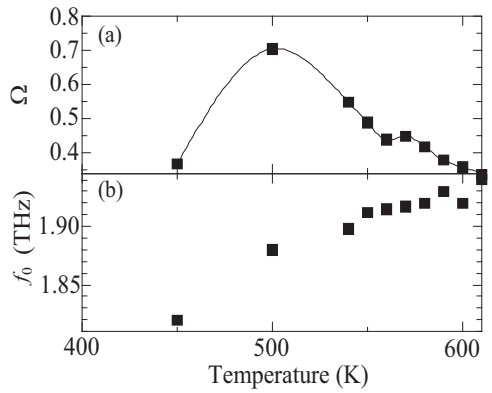

FIG. 3. Temperature dependence of (a) oscillation strength Ω, and (b) oscillation frequency f_0 of absorption band at 2 THz. The black line in (a) shows a third-order spline interpolation.

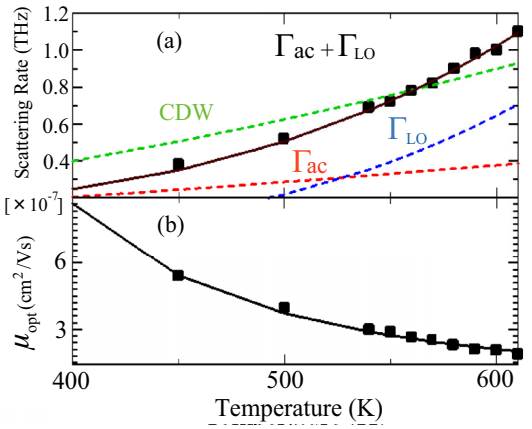

FIG. 4. (Color online) Temperature dependence of scattering rate Γ of absorption band at 2 THz. The green dotted line in (a) shows a parameter fit to a CDW model, which is proportional to a square of temperature. The red and blue dotted lines in (a) show parameter fits for an acoustic phonon scattering rate Γ_{ac} and LO phonon scattering rate Γ_{LO}. The brown line shows the sum of Γ_{ac} and Γ_{LO}. (b) Temperature dependence of the optical mobility μ_{opt}. The black line shows a parameter fit to a polaron conduction model for the mobility, which was assumed that a polaron mass is constant in whole temperature range.

revealing that Γ gradually increased with an increase of temperature. In particular, a value of Γ involves important information related to charge transport, which was fitted using the following equation related the polaron conduction [27]:

$$\Gamma_0(T) \approx \Gamma_{ac}(T) + \sum\nolimits_s \Gamma^s_{\mathrm{LO}}(T), \tag{5}$$

where $\Gamma_{ac}(T)$ and $\Gamma_{\mathrm{LO}}(T)$ indicate the acoustic phonons and longitudinal optical (LO) phonons, respectively, which can be described by the following expressions:

$$\Gamma_{ac}(T) = \frac{3\varepsilon^2_{\mathrm{def}} m^{*\frac{3}{2}}}{2\sqrt{2\pi}c_{ii}\hbar^4}(k_B T)^{\frac{3}{2}}, \tag{6}$$

$$\Gamma^s_{\mathrm{LO}}(T) = \left(\frac{m^*}{m_p}\right)^2 \frac{2\alpha_s\omega_s}{f(\alpha_s)} \exp\left(-\frac{\hbar\omega_s}{k_B T}\right), \tag{7}$$

where $\hbar$ is the Dirac constant; c_{ii}(=8294.5 kg/mm^2) [28] is the elastic constant; ω_s (=68.1 THz) is the frequency of the LO phonon modes; $\varepsilon_{\mathrm{def}}$(=22 eV) is the electron deformation potential; m_p (=0.02$m^*\alpha_s^4$) is the polaron mass, which consists of the dimensionless electron-phonon coupling constant α_s and effective mass (m^*). The function $f(\alpha_s)$ in Eq. (8) is given in Ref. [29]. It was found that temperature-dependent Γ could be fitted using Γ_0 by assuming $\alpha_s = 2.96$ and $m^* = 85.5m_0$ [Fig. 4(a)]. Here, Γ was mainly characterized by the acoustic phonon at low temperatures below 450 K [red line in Fig. 4(a)]. In contrast, the LO phonon dominated the scattering rate at high temperatures above 450 K [blue line in Fig. 4(a)]. The increased scattering rate indicated an electron-LO phonon coupling for polaron formation. In particular, α_s is one of the critical parameters describing polaron formations in various materials such as semiconductors and ionic solids. The theoretical analysis of temperature-dependent scattering rates should shed light on the nature of polaron. From the results

of parameter fits, we could obtain α_s and m^* that satisfied the following conditions: $\alpha_s < 6$ and $m_0 < m^* < m_p$ [15], providing the heavy polaron mass ($m_p = 131 m_0$).

Another feature concerning the scattering rate is the mobility (μ_{opt}) in terms of charge transport, originating from the scattering rate by the following expression: $\mu_{opt} = e/m^*\Gamma$ [Fig. 4(b)]. This parameter is determined not only by the scattering rate, but also by the effective mass m^*. Herein, we used a static value of m^* ($85.5\, m_0$) obtained by the parameter fitting based on Eq. (5) within the measurement temperatures. Temperature dependence of μ_{opt} could be understood by the following equation with activation energy E_H of 147 meV [29]:

$$\mu_{opt} \propto \exp\left[\frac{E_H}{k_B T}\right], \tag{8}$$

where μ_{opt} gradually decreased with increasing temperature, suggesting that the mobility is limited by the interaction of the carriers with LO phonons at the high temperatures. This is related to the lattice distortions around carriers, which gives rise to large polarons that are based on the Coulomb interactions between the distorted host lattices and carriers in the self-induced potential well. It is said that optical absorptions by large polarons are located in high frequency above the LO phonons. In rare-earth garnets, the frequency of lowest transverse optical (TO) phonon is close to that of the lowest LO phonon [12,25], indicating that the absorption band at 2 THz observed in a frequency below the lowest TO phonon invariably exists in a frequency below the LO phonon. In addition, large polarons lead to the Drude-like optical response because of the coherent charge motions, resulting in the formation of asymmetric spectral features. In addition, the small $\mu_{opt}(\sim 10^{-7}\,\mathrm{cm^2/V.s})$ in HoGG is very far apart from the mobility expected for the large polaron theory [30–32]. Therefore, the large polaron theory does not allow us to understand the absorption band at 2 THz.

On the other hand, optical absorptions by small polarons are derived from the interband transitions within the polaron potential well [33]. An incident light to a sample excites the carriers into a high energy state within the well from a ground state, which also forms an absorption band. In particular, a resonant frequency of an absorption band is dependent on the electron-phonon coupling constant (α_s) [33,34]. The small α_s in HoGG may allow us to observe an absorption band in the THz range in terms of small polarons. At present, we think that the absorption band at 2 THz in HoGG is related to polarons with small or intermediate polarons.

The intermediate polarons have been studied on the theoretical simulations. Thus far, some perovskites and metal oxides are referred to as intermediate polarons, where the radius of the polaron is of intermediate size. It is reported that values of α_s in intermediate polarons are in the range from 3 to 4 [35,36], which was close to that of α_s (=2.96) in HoGG.

C. Electrical transport

We studied electrical properties in order to investigate the further physical state of intermediate polarons in HoGG. Electrical resistivity ρ was measured at temperatures in the range 350 to 610 K. Interdigitated electrodes were used to detect electrical response of the sample (inset of Fig. 5).

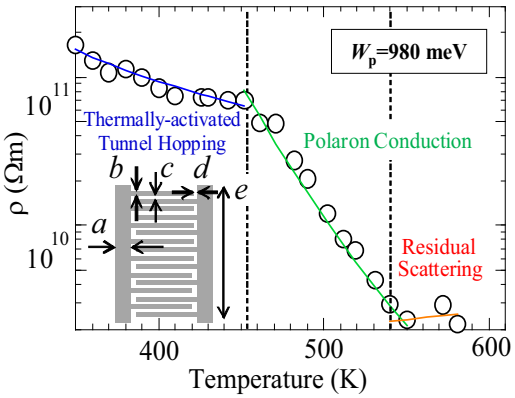

FIG. 5. (Color online) Temperature dependence of the electrical resistivity ρ. The blue, green, and red lines show fits to thermally activated tunnel hopping, polaron conduction, and residual scattering models, respectively. The inset shows the interdigitated electrodes used in the electrical measurements; the geometry of these electrodes is described by $a = 0.5$ mm, $b = 0.1$ mm, $c = 0.1$ mm, $d = 0.1$ mm, and $e = 9$ mm.

As shown in Fig. 5, three kinds of conduction mechanism were observed: (i) thermally activated tunnel hopping ρ_T, (ii) polaron conduction ρ_H, and (iii) residual scattering ρ_S. These conduction mechanisms can be expressed as follows [15,37]:

$$\rho_T = \frac{\rho_{T0}}{T}\exp\left(\frac{\Delta E}{k_B T}\right), \tag{9}$$

$$\rho_H = \rho_{H0}\exp\left(\frac{W_p}{k_B T}\right), \tag{10}$$

$$\rho_S = \rho_{S0} T^{\frac{2}{3}}, \tag{11}$$

where ΔE is the energy barrier for tunnel hopping; W_p is the activation energy; the terms ρ_{T0}, ρ_{H0}, and ρ_{S0} are empirical constants for the three conduction processes. The tunnel hopping conduction was dominant at temperatures below 450 K (blue line in Fig. 5), whereas at temperatures above 540 K, residual scattering conduction appeared to be the most important transport mechanism (orange line in Fig. 5). The polaron conduction was only activated with a W_p of 980 meV at temperature in the range 450 to 540 K (green line in Fig. 5), which was close to the theoretical calculation of intermediate polaron conduction in terms of weak electron-phonon coupling ($\alpha_s \approx 3.16$) and low carrier density [37]. Furthermore, an experimental W_p of 0.98 eV was different from a theoretical W_p of 1.67 eV, originating from ε_p (Tables I and II). Here, ε_p is sensitive to the route of sample preparation. It is reported that ε_p is larger in a polycrystalline sample than in a single crystal samples [12].

Correlation between polaron radius (r_p) and interatomic distance in conduction path plays an important role in determining a polaron type in a material. The conduction path in HoGG is related to Ga^{3+} and O^{2-} ions because electron carriers are generated from oxygen vacancies, as has been reported for $(Gd, Sc)_3Ga_5O_{12}$ [16]. The 4s orbital as a conduction path of Ga ions are much broader than the 3d orbital, which permits the hybridized orbital of Ga^{3+} and O^{2-} [38]. The interatomic distance between Ga^{3+} and O^{2-} is 0.62 Å, which is comparable

TABLE II. Polaron-related parameters for HoGG and YIG. Here, N is the number of sites per unit volume, ε_0 (=12.1) is the radio frequency (RF) relative permittivity, and ε_∞ (=3.4) is the visible light frequency relative permittivity [40,41].

Parameters	HoGG (this paper)	YIG (Ref. [39])
Lattice constant (RT), a_0 (Å)	12.282 (Ref. [39])	12.376
Debye temperature, θ_D (K)	520 (Ref. [15])	600
Elastic constant, c_{ii} (kg/mm^2)	8294.5 (Ref. [28])	7810 (Ref. [28])
Polaron dielectric constant, ε_p $\varepsilon_p = \varepsilon_\infty\varepsilon_0/[\varepsilon_0 - \varepsilon_\infty]$	4.729 (Refs. [40,41])	7.900
Polaron radius, r_p (Å) $r_p = [\pi/6N]^{1/3}/2$	0.910	0.919
Polaron binding energy, W_p (eV) $W_p = e^2/[8\pi\varepsilon_0\varepsilon_p r_p]$	1.67	0.993
Frequency of LO phonon, ω_s (THz) $\omega_s = 2\pi k_B\theta_D/h$	68.1	78.5
Polaron mass, m_p (m_e^{-1}) $m_p = 0.02m^*\alpha_s^4$	92.2	43300

to the polaron radius r_p(=0.910 Å) (Table II). The close value of the polaron radius and the conduction path produce the intermediate polaron conduction. In contrast, carrier transport in $Y_3Fe_5O_{12}$ (YIG) is clearly derived from a small polaron because the interatomic distance of conduction path between Fe ions is 5.7 Å, which is larger than a polaron radius (r_p) of 0.919 Å (Table II) [39].

The temperature range, in which small polaron conduction was electrically identified, was consistent with that observed at the absorption band at 2 THz. The oscillation strength of the absorption band was enhanced in temperature range 450 to 540 K. This indicated that small polaron conduction of carriers in the host was related to the appearance of the absorption band at 2 THz. The density of state of a carrier trapped in the well expands with an elevation of temperature, leading to the increment of the transition probability. Hopping processes of the self-trapped carriers starts around the Debye temperature ($\theta_D = 520$ K) [15]. Therefore, the absorption band at 2 THz appeared at around 450 K and then increased up to 500 K [Fig. 3(a)]. However, the oscillation strength gradually decreased in the temperature range from 500 to 600 K [Fig. 3(a)], which may be due to the residual scattering [37] from the result of electrical measurements. In general, the polaron conduction at high temperatures is limited by the residual scattering for reduction in the polaron conduction. As its origin, we consider the residual scattering as follows. There are some reports that polaron conduction is reduced at a specific temperature, which is related to a relaxed excitation state (RES) of carriers [42,43]. Trapped carriers produce polaron conduction with increasing temperature. However, existence of point defects forms short potentials in material different from the polaron mechanism [44]. As a consequence, thermally activated carriers are retrapped, resulting in that the polaron conduction was reduced with increasing temperature [44]. Our HoGG sample is polycrystalline with many defects and boundaries, which was different from ideal bulk crystals. Hereafter, we will be required to investigate single HoGG crystals from optical and electrical viewpoints. Experimental comparison between polycrystalline and bulk crystal samples will clarify polaron-related optical and electrical characteristics.

D. Other mechanisms

In Secs. III B and III C, the relationship between the optical and electrical properties indicates that the absorption band at 2 THz is related to intermediate polarons. Herein, we discuss other possibilities for explaining the formation of the absorption band at 2 THz. Absorption bands different from the usual optical phonons have been reported in the THz range for soft mode phonons [9,10], rattling phonons [45,46], resonant impurity modes [47], and CDWs [5–8].

(i) Soft mode phonons originate from a ferroelectric transition followed by structural changes [13]. $Ho_3Ga_5O_{12}$ is paraelectric at RT and shows no ferroelectric transition. Using high-temperature XRD, we confirmed that no structural transition occurred at 500 K. Furthermore, it has been reported that a resonant peak derived from the soft phonon mode shifts to lower frequencies as the temperature increases and disappears at the Curie temperature [9]. This behavior was not observed for the temperature dependence of the absorption band at 2 THz. Therefore, a soft phonon mode does not contribute significantly to the absorption band at 2 THz.

(ii) A rattling phonon mode has been observed with cagelike lattice structures [45]. This phonon mode exhibits a specific temperature dependence, i.e., the scattering rate Γ decreases with increasing temperature [46]; however, the scattering rate of the absorption band at 2 THz in HoGG increased monotonically with increasing temperature. We therefore conclude that a rattling phonon mode does not account for the absorption band at 2 THz.

(iii) A resonant impurity mode provides a sharp phonon peak caused by doping with extrinsic impurities [47]. The absorption band at 2 THz was characterized by a broad lineshape. Furthermore, SEM-EDS measurements reveal that extrinsic impurities in the samples were not present within the resolution of the instrument. Therefore, it can be concluded that resonant impurity modes are not related to the absorption band at 2 THz.

(iv) A CDW results from the collective motion of electrons in low-dimensional strongly correlated materials [6–8], providing an absorption band at THz frequencies. The scattering rate of an absorption peak due to CDW is typically proportional

to the square of temperature; however, the temperature-dependence of the scattering rate Γ in our HoGG samples [see Fig. 4(a)] cannot be fitted by the square of temperature.

From the above points, other mechanisms, such as soft phonons, rattling phonons, resonant impurities, and CDWs, are excluded as the origin of the absorption band at 2 THz. With all things considered, it is thought that the physical origin of the absorption band at 2 THz was related to an intermediate polaron conduction caused by electron carriers in HoGG, which was only operated at the high temperatures.

IV. CONCLUSION

We found the specific temperature-dependent absorption band at 2 THz in HoGG in temperature range from 450 to 540 K in addition to the contributions from optical phonons. The parameter fitting to the experimental dielectric function spectra indicated that the absorption band was related to the intermediate polaron conduction of carriers in the host. The existence of intermediate polaron conduction in HoGG was also discussed with the results of electrical measurements. This consistency between the optical and electrical measurements excluded other mechanisms resulting in formation of the absorption bands in the THz range, such as soft mode phonons, rattling phonons, impurities, and CDW modes. From the above points, it was suggested that the absorption band at 2 THz was related to intermediate polaron conduction in HoGG as identified using a THz-TDS technique.

ACKNOWLEDGMENTS

The authors would like to thank Advantest Ltd. for lending their TAS7500SP THz-TDS system. This work was supported by the Japan Society for the Promotion of Science (JSPS) Core-to-Core Program, A. Advanced Research Networks, Nanoscale Electron-Photon Interactions via Energy Dissipation and Fluctuation.

[1] M. Tonouchi, Cutting-edge terahertz technology, Nat. Photon. **1**, 97 (2007).

[2] R. Ulbricht, E. Hendry, J. Shan, T. F. Heinz, and M. Bonn, Carrier dynamics in semiconductors studied with time-resolved terahertz spectroscopy, Rev. Mod. Phys. **83**, 543 (2011).

[3] T. Kubacka, J. A. Johnson, M. C. Hoffmann, C. Vicario, S. de Jong, P. Beaud, S. Grübel, S. W. Huang, L. Huber, L. Patthey, Y. D. Chuang, J. J. Turner, G. L. Dakovski, W. S. Lee, M. P. Minitti, W. Schlotter, R. G. Moore, C. P. Hauri, S. M. Koohpayeh, V. Scagnoli *et al.*, Large-amplitude spin dynamics driven by a THz pulse in resonance with an electromagnon, Science **343**, 1333 (2014).

[4] A. Pimenov, A. A. Mukhin, V. Y. Ivanov, V. D. Travkin, A. M. Balbashov, and A. Loid, Possible evidence for electromagnons in multiferroic manganites, Nat. Phys. **2**, 97 (2006).

[5] M. Mochizuki, N. Furukawa, and N. Nagaosa, Theory of electromagnons in the multiferroic Mn perovskites: The vital role of higher harmonic components of the spiral spin order, Phys. Rev. Lett. **104**, 177206 (2010).

[6] N. Kida and M. Tonouchi, Spectroscopic evidence for a charge-density-wave condensate in a charge-ordered manganite: Observation of a collective excitation mode in $Pr_{0.7}Ca_{0.3}MnO_3$ by using THz time-domain spectroscopy, Phys. Rev. B **66**, 024401 (2002).

[7] S. Cox, J. Singleton, R. D. McDonald, A. Migliori, and P. B. Littlewood, Sliding charge-density wave in manganites, Nat. Mater. **7**, 25 (2008).

[8] A. Nucara, P. Maselli, P. Calvani, R. Sopracase, M. Ortolani, G. Gruener, M. Cestelli Guidi, U. Schade, and J. García, Observation of charge-density-wave excitations in manganites, Phys. Rev. Lett. **101**, 066407 (2008).

[9] J. Hlinka, T. Ostapchuk, D. Nuzhnyy, J. Petzelt, P. Kuzel, C. Kadlec, P. Vanek, I. Ponomareva, and L. Bellaiche, Coexistence of the phonon and relaxation soft modes in the terahertz dielectric response of tetragonal $BaTiO_3$, Phys. Rev. Lett. **101**, 167402 (2008).

[10] A. A. Sirenko, C. Bernhard, A. Golnik, A. M. Clark, J. Hao, W. Si, and X. X. Xi, Soft-mode hardening in $SrTiO_3$ thin films, Nature **404**, 373 (2000).

[11] M. Wada, K. Shirawachi, and S. Nishizawa, A fourier transform infrared spectrometer with a composite interferometer for soft mode studies, Jpn. J. Appl. Phys. **30**, 1122 (1991).

[12] M. Adachi, H. Yamahara, S. Kawabe, H. Matsui, and H. Tabata, Strong optical reflection of rare-earth garnets in the terahertz regime by reststrahlen bands, Phys. Rev. B **89**, 205124 (2014).

[13] P. C. Clapp, A localized soft mode theory for martensitic transformations, Phys. Status Solidi B **57**, 561 (1973).

[14] G. A. Sack and D. W. Oliver, Thermal conductivity of garnets and phonon scattering by rare-earth ions, Phys. Rev. B **4**, 592 (1971).

[15] I. G. Austi and N. F. Mott, Polarons in crystalline and non-crystalline materials, Adv. Phys. **50**, 757 (2001).

[16] K. B. Schwartzt and A. G. Duba, Electrical transport properties of gadolinium scandium gallium garnet, J. Phys. Chem. Solids **46**, 957 (1985).

[17] V. N. Shevchuk, V. G. Kostishin, and O. E. Bugakova, Electrical transport in $Gd_{2.6}Ca_{0.4}Mg_{0.25}Zr_{0.65}Ga_{4.1}O_{12}$ crystals $Mg_{0.25}Zr_{0.65}Ga_{4.1}O_{12}$ crystals, Inorg. Mater. **36**, 1151 (2000).

[18] P. K. Larsen and R. Metselaar, Electrical properties of yttrium iron garnet at high temperatures, Phys. Rev. B **14**, 2520 (1976).

[19] F. D'Angelo, Z. Mics, M. Bonn, and D. Turchinovich, Ultra-broadband THz time-domain spectroscopy of common polymers using THz air photonics, Opt. Express **22**, 12475 (2014).

[20] Y. J. Wu, Y. Gao, and X. M. Chen, Dielectric relaxations of yttrium iron garnet ceramics over a broad temperature range, Appl. Phys. Lett. **91**, 092912 (2007).

[21] N. T. McDevitt, Infrared lattice spectra of rare-earth aluminum, gallium, and iron garnets, J. Opt. Soc. Am. **59**, 1240 (1969).

[22] H. Zhao, J. Zhou, Y. Bai, Z. Gui, and L. Li, Infrared lattice spectra of rare-earth aluminum, gallium, and iron garnets, J. Magn. Magn. Mater. **280**, 208 (2004).

[23] Y.-J. Siao, X. Qi, C.-R. Lin, and J.-C.-A. Huang, Dielectric relaxation and magnetic behavior of bismuth-substituted yttrium iron garnet, J. Appl. Phys. **109**, 07A508 (2011).

[24] T. D. Kang, E. C. Standard, P. D. Rogers, K. H. Ahn, A. A. Sirenko, A. Dubroka, C. Bernhard, S. Park, Y. J. Choi, and S. W. Cheong, Far-infrared spectra of the magnetic exchange resonances and optical phonons and their connection to magnetic and dielectric properties of $Dy_3Fe_5O_{12}$ garnet, Phys. Rev. B **86**, 144112 (2012).

[25] K. Papagelis and S. Ves, Vibrational properties of the rare earth aluminum garnets, J. Appl. Phys. **94**, 6491 (2003).

[26] S. Anand, P. Verma, K. P. Jain, and S. C. Abbi, Vibrational properties of the rare earth aluminum garnets, Physica B **226**, 331 (1996).

[27] J. Shan, F. Wang, E. Knoesel, M. Bonn, and T. F. Heinz, Measurement of the frequency-dependent conductivity in sapphire, Phys. Rev. Lett. **90**, 247401 (2003).

[28] D. B. Sirdeshmukh, L. Sirdeshmukh, K. G. Subhadra, K. K. Rao, and S. B. Laxman, Systematic hardness measurements on some rare earth garnet crystal, Bull. Mater. Sci. **24**, 469 (2001).

[29] F. E. Low and D. Pines, Mobility of slow electrons in polar crystals, Phys. Rev. **98**, 414 (1955).

[30] H. B. Lal, B. K. Verma, and V. R. Yadav, Electrical transport in heavy rare-earth iron garnets, J. Mater. Sci. **17**, 3317 (1982).

[31] F. Iwamoto, M. Seki, and H. Tabata, Magnetic and electric properties of Ru-substituted $CoFe_2O_4$ thin films fabricated by pulsed laser deposition, J. Appl. Phys. **112**, 103901 (2012).

[32] M. Seki, H. Tabata, H. Ohta, K. Inaba, and S. Kobayashi, Epitaxial thin films of p-type spinel ferrite grown by pulsed laser deposition, Appl. Phys. Lett. **99**, 242504 (2011).

[33] D. Emin, Optical properties of large and small polarons and bipolarons, Phys. Rev. B **48**, 13691 (1993).

[34] J. Loos and J. Straka, Infrared absorption spectrum of a small-polaron system, Czech J. Phys. B **39**, 316 (1989).

[35] Y. Lépine and Y. Frongillo, Ground-state energy and effective mass of the intermediate-radius polaron in small-bandwidth polar materials, Phys. Rev. B **46**, 14510 (1992).

[36] A. A. Gogolin, The spectrum of an intermediate polaron and its bound states with phonons at strong coupling, Phys. Stat. Sol. (b) **109**, 95 (1982).

[37] S. Fratini and S. Ciuchi, Dynamical mean-field theory of transport of small polarons, Phys. Rev. Lett. **91**, 256403 (2003).

[38] E. Aubay and D. Gourier, Magnetic bistability and Overhauser shift of conduction electrons in gallium oxide, Phys. Rev. B **47**, 15023 (1993).

[39] L. Sirdeshmukh, K. K. Kumar, S. B. Laxman, A. R. Krishna, and G. Sathaiah, Dielectric properties and electrical conduction in yttrium iron garnet (YIG), Bull. Mater. Sci. **21**, 219 (1998).

[40] K. Lal and H. K. Jhans, The dielectric constant of gadolinium gallium garnet and α-Al_2O_3 single crystals, J. Phys. C: Solid State Phys. **10**, 1315 (1977).

[41] A. I. Belyaeva, A. A. Galuza, and A. D. Kudlenko, Origin of surface layer on common substrates for functional material films probed by ellipsometry, Semicond. Phys. Quantum Electron. Optoelectron. **6**, 81 (2003).

[42] W. J. Huybrechts, Internal excited state of the optical polaron, J. Phys. C: Solid State Phys. **10**, 3761 (1977).

[43] J. Devreese, J. De Sitter, and M. Goovaerts, Optical absorption of polarons in the Feynman-Hellwarth-Iddings-Platzman approximation, Phys. Rev. B **5**, 2367 (1972).

[44] B. Gerlach and H. Löwen, Analytical properties of polaron systems or: Do polaronic phase transitions exist or not? Rev. Mod. Phys. **63**, 63 (1991).

[45] H. Matsumoto, T. Mori, K. Iwamoto, S. Goshima, S. Kushibiki, and N. Toyota, Optical conductivity from local anharmonic phonons, Phys. Rev. B **79**, 214306 (2009).

[46] H. Tou, K. Sonoda, K. Furumoto, H. Kotegawa, K. Suekuni, M. A. Avila, and T. Takabatake, Strong coupling of rattling phonon to conduction electrons in semimetallic Type-I clathrate $Ba_8Ga_{16}Sn_{30}$, J. Phys. Soc. Jpn. **82**, 114603 (2013).

[47] D. Poilblanc, D. J. Scalapino, and W. Hanke, Resonant impurity scattering in a strongly correlated electron model, Phys. Rev. Lett. **72**, 884 (1994).